Characterization of mouse mediastinal fat-associated lymphoid clusters

Yaser Hosny Ali Elewa[1,2], Osamu Ichii[2], Saori Otsuka[2], Yoshiharu Hashimoto[3], Yasuhiro Kon[2,*]

[1]Department of Histology and Cytology, Faculty of Veterinary Medicine, Zagazig University, Zagazig 44519, Egypt

[2]Laboratory of Anatomy, Department of Biomedical Sciences, Graduate School of Veterinary Medicine, Hokkaido University, Sapporo 060-0818, Japan

[3]Office for International Accreditation of Veterinary Education, Obihiro University of Agriculture and Veterinary Medicine, Obihiro 080-8555, Japan

***Corresponding author**: Yasuhiro Kon, DVM, PhD, Laboratory of Anatomy, Department of Biomedical Sciences, Graduate School of Veterinary Medicine, Hokkaido University, Kita 18, Nishi 9, Kita-ku, Sapporo 060-0818, Japan. y-kon@vetmed.hokudai.ac.jp

Abstract

The association between adipose tissue and immunity has been established, and fat-associated lymphoid clusters (FALCs) are considered a source of immune cells. We discovered lymphoid clusters (LCs) in mouse mediastinal fat tissues (MFTs). In three mice strains, including Th1-biased C57BL/6N (B6), Th2-biased DBA/2Cr (DBA), and autoimmune-prone MRL/MpJ (MRL), LCs without a fibrous capsule and germinal center were observed in white-colored MFTs extending from the diaphragm to the heart. The number and size of the LCs were larger in 12-month-old mice than in 3-month-old mice in all of the examined strains. Moreover, B6 had an especially large number of LCs compared with DBA and MRL. The immune cells in the LCs consisted of mainly T-cells and some B-cells. The majority of T-cells were CD4+ helper T (Th) cells, rather than CD8+ cytotoxic T-cells, and there was no obvious immune cell population difference among three mouse strains. Furthermore, high endothelial venules and lymphatic vessels were well developed in the LCs of B6 mice than other strains. Interestingly, few CD133+ hematopoietic progenitor cells and few c-Kit+/CD127+ natural helper cells were detected in the LCs. BrdU+ proliferating cells were abundantly detected in the LCs of B6 mice compared to other strains and tended to increase with ages. This is the first report of LCs in mouse MFTs and we suggest that the size and number of LCs are affected by the mouse genetic background. We termed the LCs mediastinal fat-associated lymphoid clusters (MFALCs). These clusters may be considered niches for Th cell production.

Key words: mediastinal, adipose tissue, lymphoid cluster

Introduction

Adipose tissue is a specialized connective tissue distributed throughout the body. It acts as a cushion and stores lipids as energy sources. Furthermore, adipose tissue has been recognized as a major endocrine organ, producing hormones and adipokines such as leptin, estrogen, resistin, and tumor necrosis factor alpha (Kershaw and Flier 2004). Recently, lymphoid clusters (LCs) were observed in the adipose tissue of human and mouse mesentery; they were termed fat-associated lymphoid clusters (FALCs) (Moro et al. 2010). FALCs are in direct contact with adipocytes, lack fibrous capsules, and contain T-cells, B-cells, macrophages, and dendritic cells and are also found around the kidney and genital organs (Koyasu and Moro 2011). They are structurally similar to the milky spot in the omentum, which is considered a gateway of cells between the circulation and the peritoneal cavity (Cranshaw and Leak 1990). However, unlike the milky spot, T-cell and B-cell zones or germinal center structures are not observed in FALCs (Moro et al. 2010). Results from retinoic acid receptor-related orphan receptor gamma (RORγ)-deficient mice and alymphoplasia (aly/aly) mice suggested that the differentiation pathway of FALCs is distinct from that of lymph nodes or Peyer's patches (Nishikawa et al. 2003).

There are 2 major subsets of helper T (Th) cells, Th1 and Th2 cells, differentiated by the pattern of cytokine production (Fiorentino et al. 1989). Th1 cytokines include interleukin 2 (IL-2), IL-12, and interferon gamma (IFN-γ), which are associated with the activation of cellular immunity. Th2

54 cytokines include IL-10, IL-4, IL-5, and IL-6, which are associated with humoral immunity. In
55 addition to these Th cells, Th17 cells producing IL-17 have been identified, and these cells are
56 considered critical for the development of autoimmune disease (Bettelli et al. 2007).
57
58 The cooperation of innate and adaptive immune responses is critical for protective immunity
59 against infection (Zygmunt and Veldhoen 2011). B-cells and T-cells are the major types of cells
60 involved in the adaptive or acquired immune system. In addition to two prototypic innate
61 lymphocyte populations, namely classical natural killer (NK) and lymphoid tissue inducer (LTi) cells,
62 recent studies have identified Th2-type innate lymphocytes, such as Nh cells (Moro et al. 2010 and
63 Koyasu and Moro 2011).
64 Interestingly, such novel Th2-type innate lymphocyte, natural helper (Nh) cells express c-Kit,
65 Sca-1, interleukin-2 receptor (IL-2R), interleukin-7 receptor (IL-7R), and IL-33R were found in the
66 FALC. Nh cells in the FALC produce Th2 cytokines, including IL-5 and IL-13, and play important
67 roles in innate and anti-helminthes immunity (Moro et al. 2010). The IL-7R consists of two chains,
68 the IL-7R α-chain (IL-7Rα; also known as CD127) and the common cytokine-receptor γ-chain (γc;
69 also known as CD132) (Mazzucchelli and Durum, 2007). Recent studies revealed that CD127 is also
70 expressed by mouse natural killer (NK) lineage cells early during differentiation (Chiossone et al.
71 2009) as well as by the gut lamina propria CD56+CD3− NK cells (Takayama et al. 2010).

Autoimmune disease models such as the MRL/MpJ-lpr/lpr (MRL/*lpr*) mice develop autoantibody production, lymphadenopathy, and glomerulonephritis associated with Th1 responses, similar to human systemic lupus erythematosus. In contrast, abnormal Th2 skewing in MRL/*lpr* altered the feature of nephritis from proliferative to membranous glomerulonephritis, with an altered balance of Th1 (IFN-γ) and Th2 (IL-4) cytokine production (Shimizu et al. 2005). Shimizu et al. reported that the imbalance of Th responses is associated with autoimmune phenotypes. Interestingly, it has been reported that the genetic background of mice influences the Th responses. Briefly, mouse strains favoring a Th1 response include C57BL/6, C57BL/10, and B10.D2/nSn, and those favoring a Th2 response include DBA/2, BALB/c, BALB/cBy, BALB.B, and BALB.K (Linda et al. 2000; Charles et al. 2000). These differences in Th responses are caused by differences in the genetic background of the mice, and the susceptibility to several diseases, such as skin tumor, pneumonia, and obesity, differs between C57BL/6 and DBA/2 (Gudmundsson et al. 1998; Butler et al. 2002).

In the present study, we found LCs associating with mediastinal fat tissues (MFTs) and termed them mediastinal fat-associated lymphoid clusters (MFALCs). Furthermore, the size and lymphocyte number of the MFALCs differed among the studied mouse strains: Th1-biased C57BL/6, Th2-biased DBA/2, and autoimmune-prone MRL/MpJ. This is the first report of strain-specific differences in MFALC structures, and we hypothesize that these differences are associated with the individual characteristics of the immune responses in these strains.

90

91

Materials and methods

Experimental animals

C57BL/6N (B6), DBA/2Cr (DBA), and MRL/MpJ (MRL) mice were used in the present study. Eight- to ten-week-old mice purchased from Japan SLC (Hamamatsu, Shizuoka, Japan) were maintained with free access to specific pathogen-free food and water in our facility and were used at 3 and 12 months of age. In handling the experimental animals, the investigators adhered to the Guide for the Care and Use of Laboratory Animals, Hokkaido University, Graduate School of Veterinary Medicine (approved by the Association for Assessment and Accreditation of Laboratory Animal Care International).

Tissue preparation and microscopic observation

After euthanasia by deep inhalation anesthesia, MFTs within the mediastinum extending from the caval foramen of the diaphragm to the heart and the thymus were removed and fixed with 4% paraformaldehyde (Fig. 1). After overnight fixation, specimens were washed in distilled water, stained using the whole-mount hematoxylin method, and observed under a stereomicroscope after penetration by glycerol. For histological examination, the removed MFTs were dehydrated in graded alcohol and embedded in paraffin. Subsequently, 3-μm paraffin sections of MFT were deparaffinized, rehydrated, stained with hematoxylin and eosin (HE), and observed by light microscopy.

Immunohistochemistry

Using the MFT sections, immunohistochemical analysis for B220, BrdU, CD3, CD4, CD8, CD133, peripheral node addressin (PNAd), and lymphatic vessel endothelial hyaluronic acid receptor 1 (LYVE-1) was performed to detect B-cells, pan T-cells, Th cells, cytotoxic T (Tc) cells, hematopoietic progenitor cells (HPC), high endothelial venules (HEV), and lymphatic endothelial cells, respectively. The immunohistochemical procedures were performed according to previous reports (Elewa et al. 2010a).

The details of the antigen retrieval methods as well as the sources and dilutions of the antibodies are listed in Table 1. For the detection of proliferating cells, 5-bromo-2-deoxyuridine (BrdU) (Wako Pure Chemical Industries, Tokyo, Japan) was dissolved in PBS and injected intraperitoneally into mice at 100 mg per kg of body weight. The MFTs were removed from the animals 2 hr after BrdU injection. To detect BrdU-labeled cells, the MFT paraffin sections were stained with rat anti-BrdU antibody (Table 1). The immunopositive reactions were developed in 3,3′-diaminobenzidine-H_2O_2 solution. The sections were counterstained with hematoxylin. Sections of spleen were used as positive controls and stained by different antibodies simultaneously with the MFTs. The sections for negative controls were stained with isotype control Ig at the same concentration with the primary antibody or incubated in 0.01 M PBS without primary antibody (data not shown).

Immunofluorescence

Immunofluorescence for c-Kit and CD127 was also performed to detect the Nh cells. The deparaffinized sections were treated with 10 mM citrate buffer (pH 6.0) for 20 min at 105° C, treated with normal donkey serum, and incubated at 4° C overnight with goat anti-c-Kit antibody (1:100) and rabbit anti-CD127 antibody (1:1000) (Table 1). The sections were then incubated with Alexa Fluor 488-labeled donkey anti-goat IgG and Alexa Fluor 546-labeled donkey anti-rabbit IgG (1:500; Life Technologies) for 30 min, followed by Hoechst33342 (1:2000; Dojindo, Kumamoto, Japan) for 3 min. The immunofluorescence signals were examined by confocal microscopy.

Histoplanimetry

Light micrographs of 5 whole-mount specimens as well as paraffin sections of the MFTs from each strain were prepared for histoplanimetry. In the digital images of the sections, the areas of the LCs were observed as dark regions in the MFTs. LCs and MFTs were measured using the ImageJ software (ver. 1.32j, http://rsb.info.nih.gov/ij), and the LC-to-MFT ratio was calculated (as reported in a previous study by Elewa et al., 2010b). Based on the immunohistochemical study, the numbers of B220-, CD3-, CD4-, and CD8-positive cells in the LCs were counted in 3 different sections of the MFTs from each mouse strain. In each section, the number of immunonegative cells was also counted, and the percent of immunopositive cells among total cells was calculated as the positive

cell index for each cell population. The average of the indices for each cell population was presented.

Statistical analysis

All numerical results were shown as the mean ± standard error (SE). The results of different groups were compared using analysis of variance (ANOVA). We used the Tukey's post-hoc test for multiple comparisons when a significant difference was observed by ANOVA ($p < 0.05$).

Results

LCs in mouse MFTs

The MFTs were observed as white-colored fat tissue in the mediastinum, extending from the caval foramen of the diaphragm to the heart (Fig. 1). The localization of the MFTs was not significantly different among the examined mice (data not shown). In the stereomicroscopic observations of the whole-mount hematoxylin specimens, the examined MFTs from all mice showed dark-stained regions that varied in shape and size (Fig. 2a–f), and these regions were confirmed as LCs by subsequent histological examination (Fig. 3). In particular, the MFTs of B6 mice (Fig. 2a) had a larger number of LCs compared with DBA and MRL mice (Fig. 2b and c). The size of these LCs was also greater in C57BL/6N mice (Fig. 2d) than in other mice strains (Fig. 2e and f). These observations were confirmed by histoplanimetry (Fig. 2g); the ratios of LC area to total MFT area were significantly higher in B6 mice than in other mice strains at 3 and 12 months; notably, the values at 12 months trended higher than the values at 3 months for all examined mice.

In the HE-stained MFT sections, the dark regions of the whole-mount MFT specimens were observed as clusters of mononuclear cells (Fig 3a–f). We termed these structures MFALCs. All examined MFALCs differed from the structure of the lymph node, neither surrounded by fibrous capsules nor formed by lymphatic nodules (Fig. 3d–f). Although MFALCs were observed in all examined mice, the size and number of MFALCs were more prominent in B6 mice than in DBA and

MRL mice. Similar to the light microscope observations of the HE-stained MFT sections, the histoplanimetrical measurements of the ratio of the LC area to the total MFT area (Fig. 3g) revealed a significantly greater ratio in B6 mice than in other mice at 3 and 12 months. In addition, the values at 12 months trended higher than the values at 3 months for all examined mice.

Blood vessels and lymphatic vessels in mouse MFALCs

As a characteristic of MFALCs, blood capillaries and venules were observed within the LCs (Fig. 3e and Fig. 4), and several lymphocytes and red blood cells were observed in their lumens. Some endothelial cells in the venules of the MFALCs had abundant cytoplasms and large nuclei, characteristics of HEVs (Fig. 4a and b). Based on the immunohistochemical analysis of PNAd (HEV marker), the endothelial cells of the venules of the MFALCs showed positive reactions, and the positive reactions were stronger in B6 mice (Fig. 4c) than in DBA and MRL mice (Fig. 4d and e) at 12 months. No positive reaction in HEV was observed in the serial sections stained with normal IgM controls (Fig. 4f- h).

Furthermore, lymphatic vessels positive for LYVE-1 were observed within the MFALCs (Fig. 5a-b) as well as the mediastinal fat tissue (Fig. 5c-f), whereas blood vessels containing erythrocytes were not positive for LYVE-1 (Fig. 5c). Interestingly, these lymphatic vessels were abundantly observed in B6 mice (Fig. 5a-c) compared to DBA (Fig. 5d) and MRL mice (Fig. 5e and f) at 12

months.

Immune cells in mouse MFALCs

To determine the population of immune cells in the MFALCs, immunohistochemical analysis of B220, CD3, CD4, and CD8 was performed to detect B-cells, pan T-cells, Th cells, and Tc cells, respectively. In three strains, B220-positive B-cells and CD3-positive T-cells were observed; the latter was more predominantly observed than the former (Fig. 6a, b, e, and f). For T-cells, CD4-positive Th cells (Fig. 6c and g) were more abundant than CD8-positive Tc cells (Fig. 6d and h). These results were confirmed by histoplanimetry. The immunopositive cell index of CD3 was higher than for other markers in all examined mice, and the index of CD4 was higher than that of CD8 (Fig. 6i). No significant strain-specific difference was observed in the populations of MFALC immune cells. Furthermore, few F4/80-positive cells were detected in the MFALC, and no significant strain difference was observed (data not shown).

For all examined strains, few CD133-positive cells were observed in the MFALCs (Fig. 7), and these cells were localized within large-sized LCs (Fig. 7a), the lumen of blood vessels (Fig. 7b and c), and small-sized LCs (Fig. 7b and d). The mononuclear cells in the small-sized LCs (Fig. 7b) appeared to be newly aggregated, containing more CD133-positive cells than mononuclear cells in the large-sized LCs (Fig. 7a). No positive cells were observed in the serial sections stained with

normal IgG controls (Fig. 7e and f).

Immunofluoresence revealed the presence of few c-Kit^{+}/CD127^{+} cells and many c-Kit^{-}/CD127^{+} cells within the MFALC of C57BL/6 at ** months (Fig. 8a-d). These results were also confirmed by immuhohistochemistry for c-Kit and CD127 (Supplementary figure 1a and b).

BrdU-positive cells were observed in the MFALC (Fig. 9). Numerous BrdU-positive cells were observed within the MFALC of B6 mice (Fig. 9c and f) than DBA mice (Fig. 9a and d) at 12 months. Moreover, numerous number of BrdU-positive cells was observed in the MFALC of B6 mice at 12 months (Fig. 9c and f) than that at 3 months (Fig. 9b and e).

Discussion

LCs in the MFTs

Adipose tissue is no longer considered an inert tissue that solely functions in energy storage. Other important roles of adipose tissue are emerging, for example, the regulation of various physiological and pathological processes. Recently, there has been much effort to define the roles of adipokine-soluble mediators derived mainly from adipocytes in the interactions between adipose tissues and immunity (MacLaren et al. 2008). Adiponectin and leptin have emerged as the most abundant adipokines produced by adipocytes, thereby redefining adipose tissue as a key component of the endocrine and immune systems (Tilg and Moschen 2006).

Novel LCs called FALCs were discovered in the mesenteric adipose tissue of humans and mice (Moro et al. 2010). In the present study, we focused our examination of mouse MFTs at 3 and 12 months, corresponding to early and late adulthood, respectively. We discovered LCs in the MFTs of the mouse mediastinum extending from the caval foramen of the diaphragm to the heart. Our histological examinations revealed that these LCs had no fibrous capsules and contained more T-cells than B-cells. Therefore, the structural characteristics and immune cell populations of the MFALCs are similar to the mesenteric FALCs (Moro et al. 2010). Furthermore, the border between the T-cell and B-cell areas was unclear, and no germinal center was observed in the LCs of the mouse MFTs, unlike the milky spot in the omentum (Cranshaw and Leak 1990). The LCs of the

246 MFTs were observed in healthy B6 and DBA mice as well as autoimmune-prone MRL mice. These
247 morphological characteristics and the appearance of MFALCs in healthy mice differed from the
248 tertiary lymphoid follicles and LCs present in the target tissues of various immune diseases, such as
249 synovial tissue in rheumatoid arthritis (Takemura et al. 2001). From these findings, the lymphoid
250 structures that we discovered in the mouse MFTs were clearly distinct from lymphatic nodules and
251 pathological cell infiltrations and were universally observed in different mouse strains. We termed
252 these clusters MFALCs.
253
254 *Age- and strain-specific differences in MFALCs caused by different genetic backgrounds*
255 The putative functions of mouse mesentery FALCs are the self-replication of peritoneal B-cells,
256 the induction of IgA production, and the promotion of an antiparasitic response via Th2 cytokines of
257 Nh cells (Moro et al. 2010; Koyasu et al. 2010; Koyasu and Moro 2011). However, the proper
258 functions of MFALCs in mice and their presence in humans are still unknown. Importantly, in this
259 study, strain- or age-specific changes in MFALCs were observed in mice, and the size of MFALCs
260 increased with age. Age-related changes in immune cells are important for the response to antigen.
261 Briefly, the number of splenic myeloid dendritic cells was higher in middle-aged (8-month-old) and
262 young (3-week-old) B6 mice, and these age-dependent differences in dendritic cells were associated
263 with resistance to *Plasmodium* infection in middle age (Shan et al. 2012). In calves, total mucosal

264 leukocytes increased with age in the small intestine; much of this increase was attributed to mucosal
265 CD3+ T-cells. In particular, CD4+ T-cells increased significantly in the jejunum, and CD8+ T-cells
266 increased significantly with age throughout the small intestine (Fries et al. 2011). Furthermore,
267 age-dependent development of the duct-associated lymphoid tissue (DALT) of minor salivary glands
268 was reported in *Macaca fascicularis* (crab-eating macaque); DALT may play a substantial role in the
269 local immunosurveillance of the oral cavity (Nair et al. 1987). These findings suggest the age-related
270 differences in MFALCs might be associated with some immunological functions, relating to
271 increased host responses to pathogens and native antigens.

272 Furthermore, the mouse strain-specific differences were clarified by examination of MFALC
273 morphology. Briefly, the ratio of MFALC area to MFT area was significantly higher in B6 mice than
274 in DBA mice and autoimmune-prone MRL mice. Interestingly, Th1-biased B6 mice are susceptible
275 to hypersensitive pneumonitis, but Th2-biased DBA mice are resistant to it (Butler et al. 2002;
276 Gudmundsson et al. 1998). Hypersensitive pneumonitis is a granulomatous inflammatory lung
277 disease caused by repeated inhalation of organic antigens in humans and mice (Fink 1992; Sharma
278 and Fujimura 1995). Although exposure to pathogenic antigens is widespread in humans, only a
279 minority (5–10%) of the exposed individuals develop clinical disease (Fink 1992), and variations in
280 the susceptibility to hypersensitive pneumonitis, due, for example, to genetic background, might
281 contribute to these differences in humans as well as other animals. Furthermore, eosinophilic

macrophage pneumonia is observed more frequently in mice with the B6 genetic background (Murray and Luz 1990; Hoenerhoff et al. 2006). In addition to lung diseases, the genetic background of B6 mice may be associated with aseptic inflammation of the upper urinary tract, which accelerates the pathological effects of the MRL -derived autoimmune susceptibility locus for glomerulonephritis (Ichii et al. 2008; Ichii et al. 2011). Therefore, strain-specific differences in MFALC areas may underlie the differential immune response, mediated by several genetic factors. In particular, the Th1-biased B6 background might be associated with the acceleration of susceptibility to intrapleural disease.

Structural characteristics of MFALCs

In the histological examination, we clarified that the majority of the immune cells in the MFALCs were T-cells, rather than B-cells, and specifically CD4-positive Th cells, rather than CD8-positive Tc cells. There were no strain-specific differences in these populations. The mesenteric FALCs also contain CD3-positive T-cells and B220-positive B-cells (Moro et al. 2010). The mesenteric FALCs also contain Th2-type innate lymphocytes called Nh cells (c-Kit$^+$, Sca-1$^+$, IL-2$^+$, IL-2R$^+$, IL-7R$^+$, and IL-33R$^+$) (Moro et al. 2010). Similarly, our results revealed the presence of c-Kit$^+$/CD127$^+$ cells, and we suggested that the MFALCs contained Nh cells. Furthermore, we detected numerous c-Kit-/CD127+cells within the MFALCs. Chiossone et al. 2009 reported that

CD127 is also expressed by mouse natural killer cells (NK) lineage cells early during differentiation. Thus, our finding of numerous $CD127^+$ cells within the MFALCs suggest that the MFALCs could be also a source of NK cells.

Interestingly, we found blood vessels, such as blood capillaries and venules, in the MFALCs of all examined mice, and the venules showed positive reactions for an HEV marker, PNAd. These PNAd-positive venules were more prominent in B6, which had the largest MFALC area among the examined mouse strains. Lymphocytes are intrinsically mobile; they circulate continuously between the blood and secondary lymphoid tissues. When naive lymphocytes first enter the lymph nodes and Peyer's patches, they adhere to and migrate across the HEV (Kraal and Mebius 1997; Miyasaka and Tanaka 2004). Moreover, LYVE-1-positive lymphatic vessels were observed within the MFALCs and the MFTs. Such lymphatic vessels were more prominent in B6 mice than other examined strains suggesting the major role of lymph vessels for lymphocyte emigration and antigen transport.

Furthermore, we found that some CD133-positive cells were observed in the LCs or the lumen of the blood vessels in the MFALCs, indicating the presence of HPCs (Handgretinger and Kuçi 2013). It has been suggested that the migration of hematopoietic stem cells occurs through the blood, across the endothelial vasculature, to different organs and to their bone marrow niches via a homing process (Lapidot et al. 2005). From these findings, we propose that immature hematopoietic cells migrate to MFALCs via HEV and act as niches for Th cell production.

Our results revealed the presence of BrdU-positive cells within the clusters, indicating that some proliferating cells are present in the MFALCs (Taupin 2007). Our results revealed that numerous BrdU-positive cells were observed in the B6 mice compared to other strains. Moreover, the number of BrdU-positive cells tended to increase with ages. Fulton et al. (2010) showed that regulatory T-cells (Treg) incorporating BrdU rapidly accumulate in the lung-draining mediastinal lymph nodes and lungs following acute respiratory syncytial virus infection. Furthermore, Mannering et al. (2002) revealed that *Listeria* infection causes a dramatic and acute activation and proliferation of T-cells. The present study revealed that normal MFALC structures contain T-cells, B-cells, hematopoietic cells, and proliferating cells in healthy mice. Further studies are required to characterize the immune responses in MFALCs in mice challenged with foreign antigens, focusing especially on the T regulatory response.

Acknowledgements

This work was supported by the Partnership and Ownership Initiative (ParOwn), which was funded by the Egyptian Ministry of Higher Education and the State for Scientific research. The work was also supported by a Grant-in-Aid for Scientific Research B (No. 24380156) from the Ministry of Education, Culture, Sports, Science, and Technology of Japan.

References

Bettelli E, Oukka M, Kuchroo VK (2007) TH-17 cells in the circle of immunity and autoimmunity. Nat Immunol 8: 345-350

Butler NS, Monick MM, Yarovinsky TO, Powers LS, Hunninghake GW (2002) Altered IL-4 mRNA stability correlates with Th1 and Th2 bias and susceptibility to hypersensitivity pneumonitis in two inbred strains of mice. J Immunol 169: 3700-3709

Charles DM, Kristi K, Jennifer MA, Michelle J (2000) M-1/M-2 macrophages and the Th1/Th2 paradigm. J Immunol 164: 6166-6173

Chiossone L, Chaix J, Fuseri N, Roth C, Vivier E, Walzer T (2009) Maturation of mouse NK cells is a 4-stage developmental program. Blood 113: 5488–5496.

Cranshaw ML, Leak LV (1990) Milky spots of the omentum: a source of peritoneal cells in the normal and stimulated animal. Arch Histol Cytol 53: 165-177

Elewa YH, Bareedy MH, Abuel-Atta AA, Ichii O, Otsuka S, Kanazawa T, Lee SH, Hashimoto Y, Kon Y (2010a) Cytoarchitectural differences of myoepithelial cells among goat major salivary glands. Vet Res Commun 34: 557-567

Elewa YH, Bareedy MH, Abuel-Atta AA, Ichii O, Otsuka S, Kanazawa T, Lee SH, Hashimoto Y, Kon Y (2010b) Structural characteristics of goat *(Capra hircus)* parotid salivary glands. Jpn J Vet Res 58: 121-135

354 Fink JN (1992) Hypersensitivity pneumonitis. Clin Chest Med 13: 303-309

355 Fiorentino DF, Bond MW, Mosmann TR (1989) Two types of mouse T-helper cell. IV. Th2 clones

356 secrete a factor that inhibits cytokine production by Th1 clones. J Exp Med 170: 2081-2095

357 Fries PN, Popowych YI, Guan LL, Griebel PJ (2011) Age-related changes in the distribution and

358 frequency of myeloid and T cell populations in the small intestine of calves. Cell Immunol 271:

359 428-437

360 Fulton RB, Meyerholz DK, Varga SM (2010) Foxp3^{+} CD4 regulatory T cells limit pulmonary

361 immunopathology by modulating the CD8 T cell response during respiratory syncytial virus

362 infection. J Immunol 185: 2382-2392

363 Gudmundsson G, Monick MM, Gary W (1998) IL-12 modulates expression of hypersensitivity

364 pneumonitis. J Immunol 161: 991-999

365 Handgretinger R, Kuçi S (2013) CD133-positive hematopoietic stem cells: from biology to medicine.

366 Adv Exp Med Biol 777: 99-111

367 Hoenerhoff MJ, Starost MF, Ward JM (2006) Eosinophilic crystalline pneumonia as a major cause of

368 death in 129S4/SvJae mice. Vet Pathol 43: 682-688

369 Ichii O, Otsuka S, Namiki Y, Hashimoto Y, Kon Y (2011) Molecular pathology of murine ureteritis

370 causing obstructive uropathy with hydronephrosis. PLoS ONE 6: e27783

371 Ichii O, Konno A, Sasaki N, Endoh D, Hashimoto Y, Kon Y (2008) Autoimmune glomerulonephritis

induced in congenic mouse strain carrying telomeric region of chromosome 1 derived from MRL/MpJ. Histol Histopathol 23: 411-422

Kershaw EE, Flier JS (2004) Adipose tissue as an endocrine organ. J Clin Endocrinol Metab 89: 2548-2556

Koyasu S, Moro K (2011) Type 2 innate immune responses and the natural helper cell. Immunology 132: 475-481

Koyasu S, Tanabe M, Takeuchi T, Moro K (2010) Natural helper cells: a new player in the innate immune response against helminth infection. Adv Immunol 108: 21-44

Koyasu S, Moro K (2011) Innate Th2-type immune responses and the natural helper cell, a newly identified lymphocyte population. Curr Opin Allergy Clin Immunol 11: 109–114

Kraal G, Mebius RE (1997) High endothelial venules: lymphocyte traffic control and controlled traffic. Adv Immunol 65: 347-395

Lapidot T, Dar A, Kollet O (2005) How do stem cells find their way home? Blood J 106: 1901-1910

Linda DH, Sharon MC, Byungsuk K, Ronald B (2000) Increased severity of pseudomonas aeruginosa corneal infection in strains of mice designated as Th1 versus Th2 responsive. Invest Ophthalmol Vis Sci 41: 805-810

MacLaren R, Cui W, Cianflone K (2008) Adipokines and the immune system: an adipocentric view. Adv Exp Med Biol 632: 1-21

390 Mannering SI, Zhong J, Cheers C (2002) T-cell activation, proliferation and apoptosis in primary
391 Listeria monocytogenes infection. Immunology 106: 87-95
392 Mazzucchelli R, Durum SK (2007) Interleukin-7 receptor expression: intelligent design. Nature
393 Reviews Immunology 7:144-154
394 Miyasaka M, Tanaka T (2004) Lymphocyte trafficking across high endothelial venules: dogmas and
395 enigmas. Nat Rev Immunol 4: 360-370
396 Moro K, Yamada T, Tanabe M, Takeuchi T, Ikawa T, Kawamoto H, Furusawa J, Ohtani M, Fujii H,
397 Koyasu S (2010) Innate production of TH2 cytokines by adipose tissue-associated c-Kit^{+}Sca-1^{+}
398 lymphoid cells. Nature 463: 540-544
399 Murray AB, Luz A (1990) Acidophilic macrophage pneumonia in laboratory mice. Vet Pathol 27:
400 274-281
401 Nair PN, Zimmerli I, Schroeder HE (1987) Minor salivary gland duct-associated lymphoid
402 tissue (DALT) in monkeys changes with age. J Dent Res 66: 407-411
403 Nishikawa S, Honda K, Vieira P, Yoshida H (2003) Organogenesis of peripheral lymphoid organs.
404 Immunol Rev 195: 72-80
405 Shan Y, Liu J, Jiang YJ, Shang H, Jiang D, Cao YM (2012) Age-related susceptibility and resistance
406 to nonlethal Plasmodium yoelii infection in C57BL/6 mice. Folia Parasitol (Praha) 59: 153-161
407 Sharma OP, Fujimura N (1995) Hypersensitivity pneumonitis: a noninfectious granulomatosis.

408 Semin Respir Infect 10: 96-106

409 Shimizu S, Sugiyama N, Masutani K, Sadanaga A, Miyazaki Y, Inoue Y, Akahoshi M, Katafuchi R,

410 Hirakata H, Harada M, Hamano S, Nakashima H, Yoshida H (2005) Membranous

411 glomerulonephritis development with Th2-type immune deviations in MRL/lpr mice deficient for

412 IL-27 Receptor (WSX-1). J Immunol 175: 7185-7192

413 Takayama T, Kamadax N, Chinen H et al. (2010) Imbalance of NKp44(+) NKp46(-) and NKp44(-)

414 NKp46(+) natural killer cells in the intestinal mucosa of patients with Crohn's disease.

415 Gastroenterology 139: 882–892

416 Takemura S, Braun A, Crowson C, Kurtin PJ, Cofield RH, O'Fallon WM, Goronzy JJ, Weyand CM

417 (2001) Lymphoid neogenesis in rheumatoid synovitis. J Immunol 167: 1072-1080

418 Taupin P (2007) BrdU immunohistochemistry for studying adult neurogenesis: paradigms, pitfalls,

419 limitations, and validation. Brain Res Rev 53: 198-214

420 Tilg H, Moschen AR (2006) Adipocytokines: mediators linking adipose tissue, inflammation and

421 immunity. Nat Rev Immunol 6: 772-783

422 Zygmunt B, Veldhoen M (2011) T helper cell differentiation more than just cytokines. Adv

423 Immunol 109: 159–196

424

425 **Figure legends**

426 **Fig. 1** Gross anatomical localization of mediastinal fat tissue (MFT) in mice: White-colored MFT
427 (arrows) extending from the diaphragm (D) to the heart (H). DBA/2Cr mouse, 12 months. C: chest
428 including sternum and ribs. T: thymus

429

430 **Fig. 2** Mediastinal fat-associated lymphoid clusters in mice. Panels a–f show the stereomicroscopic
431 photographs of whole-mount hematoxylin-stained mediastinal fat tissues (MFTs) from C57BL/6N
432 (panels A and D), DBA/2Cr (panels B and E), and MRL/MpJ (panels C and F) mice at 12 months.
433 The squares in panels a–c indicate the same areas as those in panels d–f. In each panel, the
434 dark-stained regions represent the lymphoid clusters (LCs) of the MFT (panels d–f, arrows). Larger
435 numbers and areas of LCs are visible in C57BL/6N mice (panels a and d) compared with DBA/2Cr
436 (panels b and e) and MRL/MpJ (panels c and f) mice. (g) Percentage of LC area in the total MFT
437 area in the hematoxylin whole-mount specimens. D and M: Significant differences between
438 DBA/2Cr (D) and MRL/MpJ (M) mice, analyzed by Tukey's post-hoc test subsequent to ANOVA (p
439 < 0.05); $n \geq 3$ mice of each strain (at 3 months n = 5, 3, 3 and at 12 months n = 5, 5, 5 in C57BL/6N,
440 DBA/2Cr, and MRL/MpJ mice, respectively). Values are given as the mean ± SE

441

442 **Fig. 3** Histological features of mediastinal fat-associated lymphoid clusters in mice. Panels a–f show

443 light microscope photographs of hematoxylin and eosin (HE)-stained mediastinal fat tissue (MFT)
444 sections of C57BL/6N (panels a and d), DBA/2Cr (panels b and e), and MRL/MpJ (panels c and f)
445 mice at 12 months. The squares in panels a–c indicate the same areas as those in panels d–f. In each
446 panel, the accumulation of mononuclear cells is visible in the MFT (panels d–f). More lymphoid
447 clusters (LCs) with larger areas are visible in C57BL/6N mice (panels a and d) compared with
448 DBA/2Cr and MRL/MpJ mice. (g) Percentage of LC area in the total MFT area in the HE-stained
449 sections. D and M: Significant differences between DBA/2Cr (D) and MRL/MpJ (M), analyzed by
450 Tukey's post-hoc test subsequent to ANOVA ($p < 0.05$); $n \geq 3$ mice of each strain (at 3 months n = 5,
451 4, 3 and at 12 months n = 4, 4, 4 in C57BL/6N, DBA/2Cr, and MRL/MpJ mice, respectively). Values
452 are given as the mean ± SE
453
454 **Fig. 4** Blood vessels in mediastinal fat-associated lymphoid clusters (MFALCs) in mice. Panels a
455 and b show light microscope photographs of hematoxylin and eosin (HE)-stained mediastinal fat
456 tissue (MFT) sections of C57BL/6N mice at 12 months. Large blood vessels containing lymphocytes
457 (arrowheads) are visible (panel a). In the MFALCs, the endothelial cells of the vessels show
458 epithelioid features with abundant cytoplasms and large nuclei (panels a and b). The squares in panel
459 a indicate the same areas as those in panel b. Panels c–e show light microscope photographs of
460 immunohistochemical stains for the high-abundance endothelial venules marker PNAd in C57BL/6N

(panel c), DBA/2Cr (panel d), and MRL/MpJ mice (e) at 12 months. PNAd-positive endothelial cells are visible in the venules of the MFALCs in all of the examined mice (panels c–e, arrows). Panels f–h show the serial section of panels c-e stained by normal rat IgM instead of anti-PNAd antibody, and no normal IgM-positive reaction is observed in the venules.

Fig. 5 Lymphatic vessels in mediastinal fat-associated lymphoid clusters in mice. Panels a–f show light microscope photographs of immunohistochemical stains for the lymphatic vessels marker LYVE-1 in C57BL/6N (panels a–c), DBA/2Cr (panel d), and MRL/MpJ mice (e and f) at 12 months. The solid and dotted squares in panel a indicate the same areas as those in panel b and c respectively. LYVE-1-positive lymph vessels are clearly observed in the mediastinal fat tissues (MFTs) (panel b and c, Lv). Erythrocyte-filled blood vessel (panel c, Bv) is negative for LYVE-1. The square in panel e indicate the same area as that in panel f. LYVE-1-positive lymphatic vessels were well developed in the MFTs of C57BL/6N mice (panels a–c) than those of DBA/2Cr mice (panel d) and MRL/MpJ mice (e and f).

Fig. 6 Immune cell populations of mediastinal fat-associated lymphoid clusters (MFALCs) in mice. Panels a–h show light microscope photographs of immunohistochemical stains for B220 (B-cells, panels a and e), CD3 (pan T-cells, panels b and f), CD4 (helper T-cells, panels c and g), and CD8

(cytotoxic T-cells, panels d and h) in C57BL/6N mice at 12 months. The squares in panels a–d indicate the same areas as those in panels e–h. Cells immunopositive for each antigen are visible in the MFALC of C57BL/6N mice. (i) Index of immune cell populations in the MFALCs of the mice. a, b, c, and d: Significant differences between B220 (a), CD3 (b), CD4 (c), and CD8 (d) in same mouse strain, m: Significant difference with MRL/MpJ in same antigen, analyzed by Tukey's post-hoc test subsequent to ANOVA ($p < 0.05$); n = 3 mice in each strain. Values are given as the mean ± SE

Fig. 7 CD133-positive cells of mediastinal fat-associated lymphoid clusters (MFALCs) in mice. Panels a–d show light microscope photographs of immunohistochemical stains for CD133 (marker for hematopoietic progenitor cells)-positive cells in C57BL/6N mice at 12 months. The dotted and solid squares in panel b indicate the same areas as those in panel c and d respectively. Few positive cells are visible in the MFALC (panel a, arrows) and in the lumen of the MFALC vessels (v) (panel b and c). In panel d, the smaller-sized lymphoid clusters showed numerous CD133-positive cells. Panels e and f are stained by normal rabbit IgG instead of anti-CD133 antibody for negative control, and the square in panel e indicate the same area as those in panel f. No normal IgG-positive cells were observed in the MFALC (Panels 7e and f).

Fig. 8 c-Kit- and CD127-positive cells of mediastinal fat-associated lymphoid clusters (MFALCs) in

497 mice. Panels are representative images of immunofluoresce for c-Kit (panel a, green) and CD127
498 (panel b, red) with nuclear staining by Hoechst (panel c, blue) in C57BL/6 at ** months. Merged
499 image is shown in panel d, demonstrating the presence of few c-Kit+/ CD127+ cells (arrows) and
500 many c-Kit-/ CD127+ cells within the MFALC.
501
502 Fig. 9 Proliferating cells in the mediastinal fat-associated lymphoid clusters (MFALCs) in mice.
503 Proliferating cells were detected by immunohistochemistry for BrdU in DBA/2Cr at 12 months
504 (panel a) and C57BL/6N mice at 3 and 12 months (panels b and c respectively). Panels d, e and f are
505 higher magnification to the square area in panels a, b and c respectively. Note fewer BrdU-positive
506 cells are visible within the MFALCs in DBA/2Cr mice (panel a and d) compared to C57BL/6N mice
507 (panels b and e) at 12 months. Interestingly, in C57BL/6N mice, BrdU-positive cells are abundantly
508 observed at 12 months (panels b and e) compared to 3 months (panels c and f).

Figure 1.

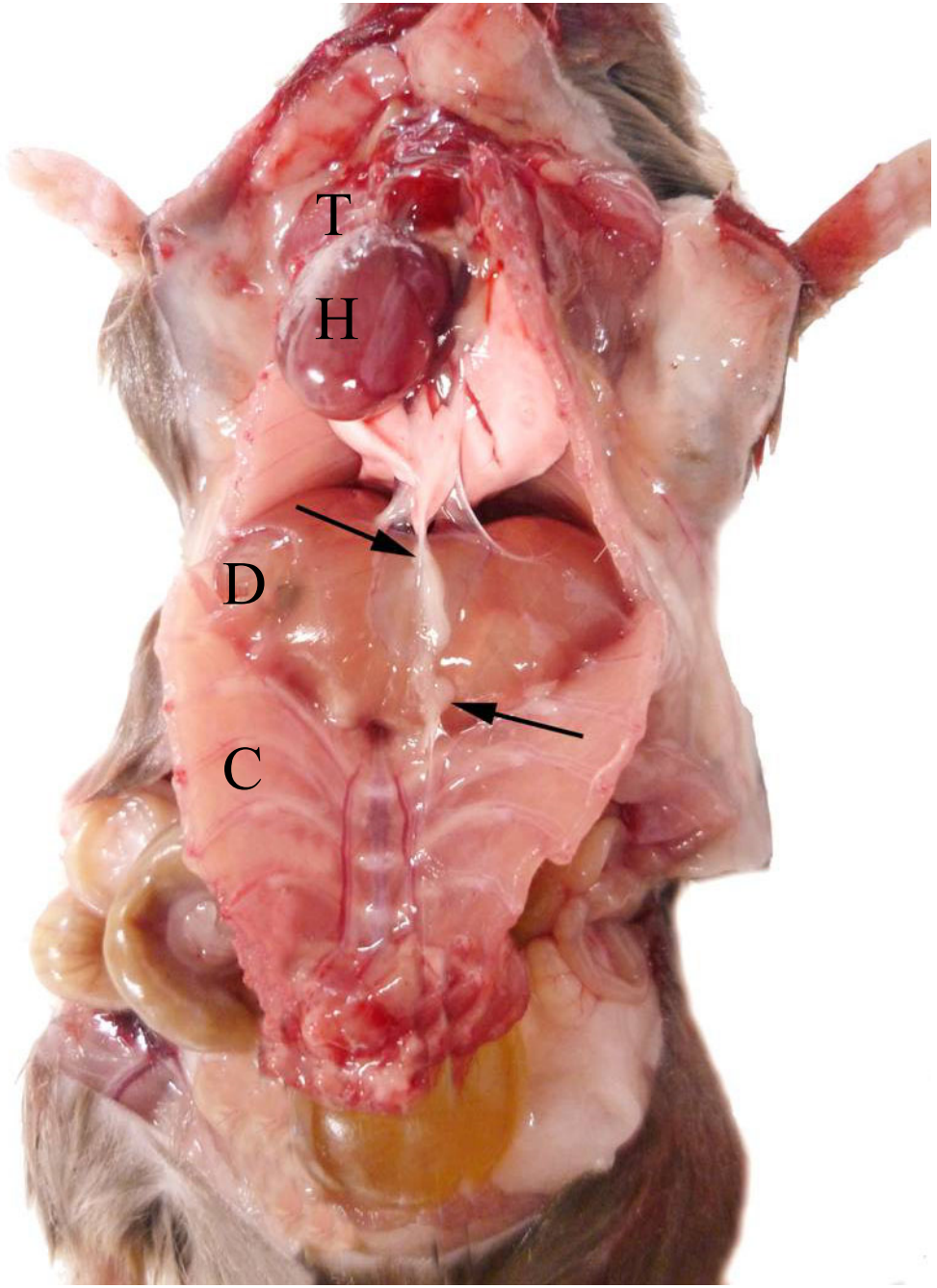

Figure 2.

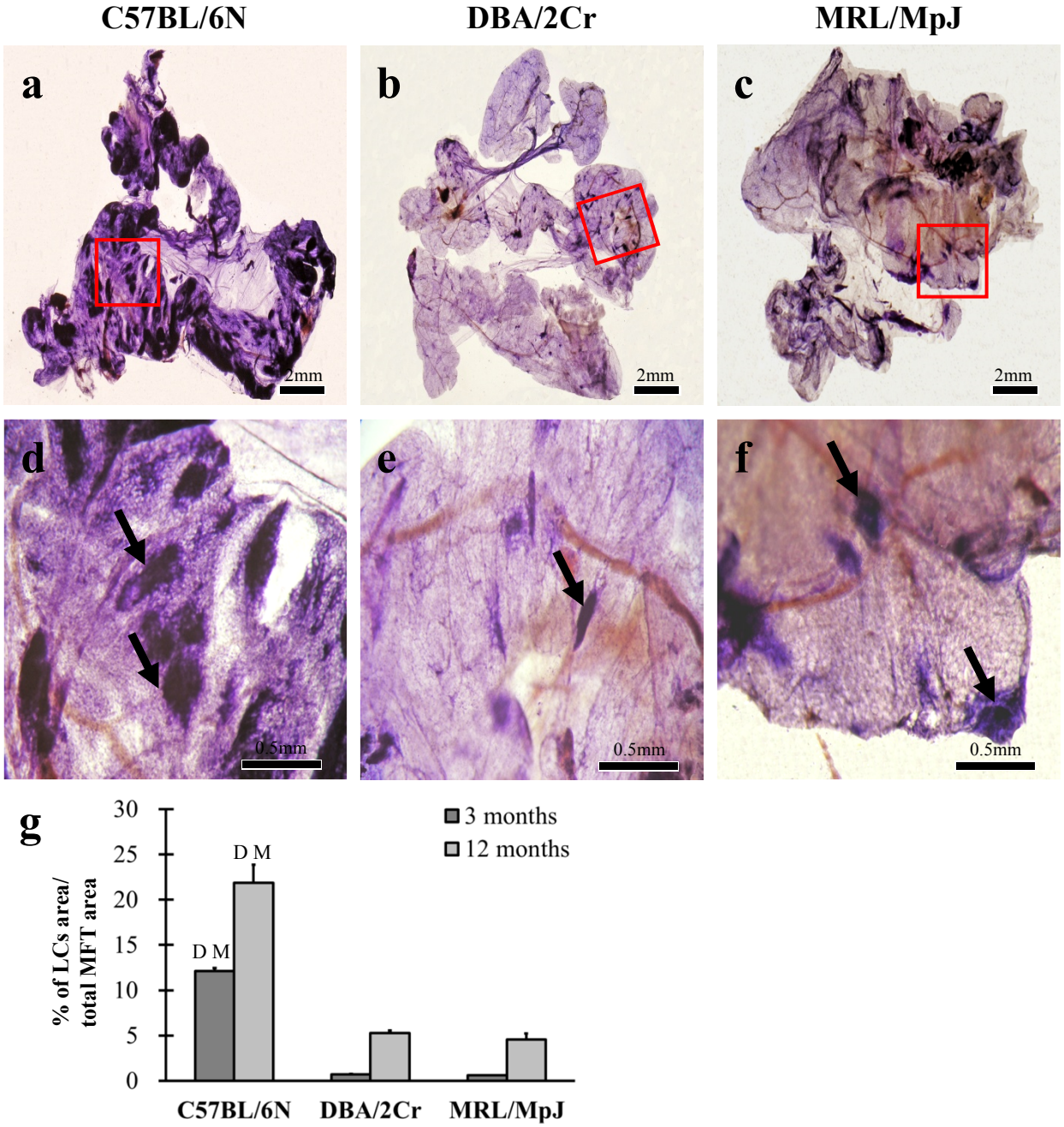
C57BL/6N
DBA/2Cr
MRL/MpJ
a
b
c
2mm
2mm
2mm
d
e
f
0.5mm
0.5mm
0.5mm
g
3 months
12 months
% of LCs area/ total MFT area
30
25
20
15
10
5
0
D M
D M
C57BL/6N
DBA/2Cr
MRL/MpJ

Figure 3.

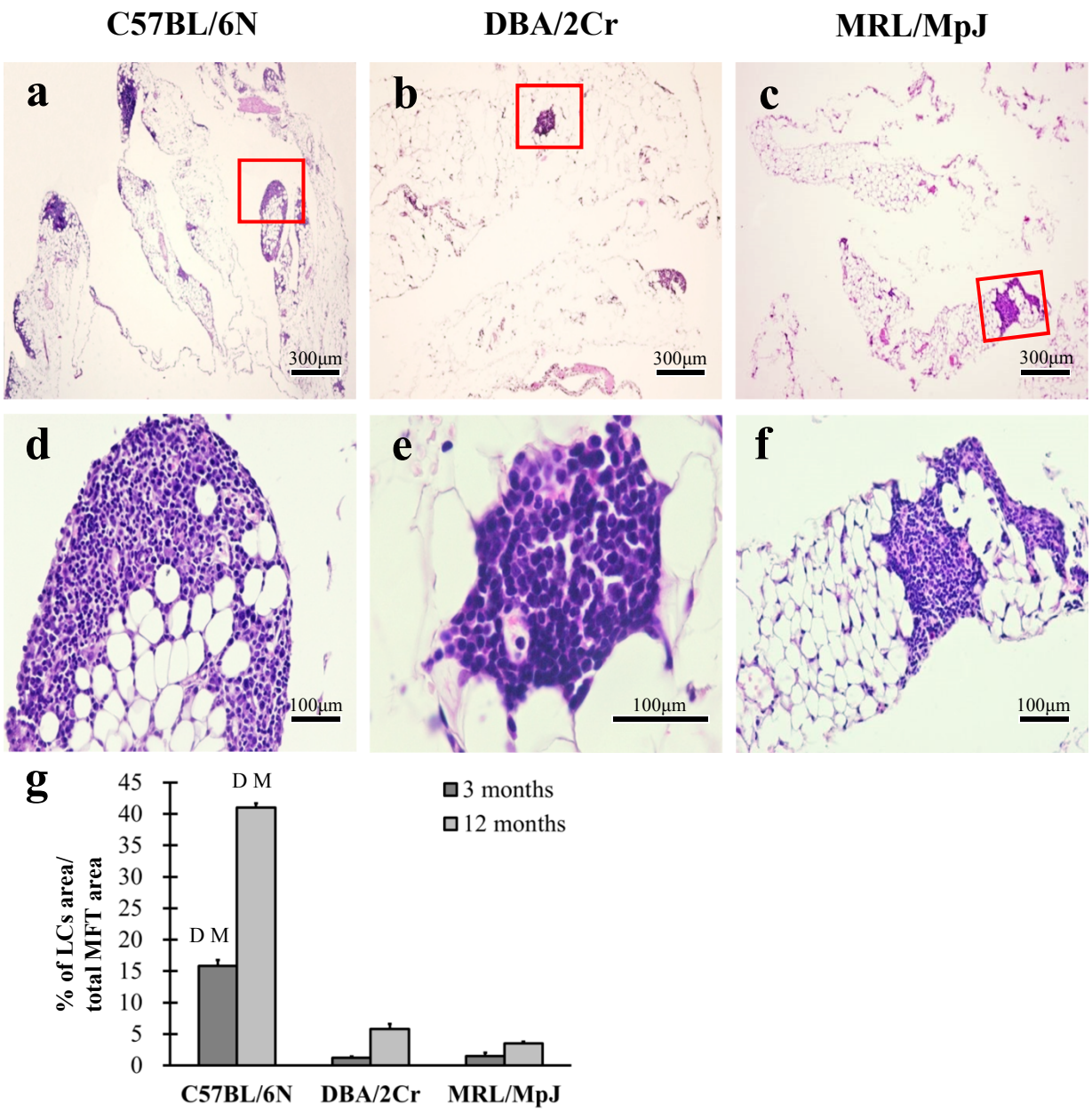
C57BL/6N
DBA/2Cr
MRL/MpJ
a
b
c
300μm
300μm
300μm
d
e
f
100μm
100μm
100μm
g
% of LCs area/ total MFT area
45
40
35
30
25
20
15
10
5
0
D M
D M
3 months
12 months
C57BL/6N
DBA/2Cr
MRL/MpJ

Figure 4.

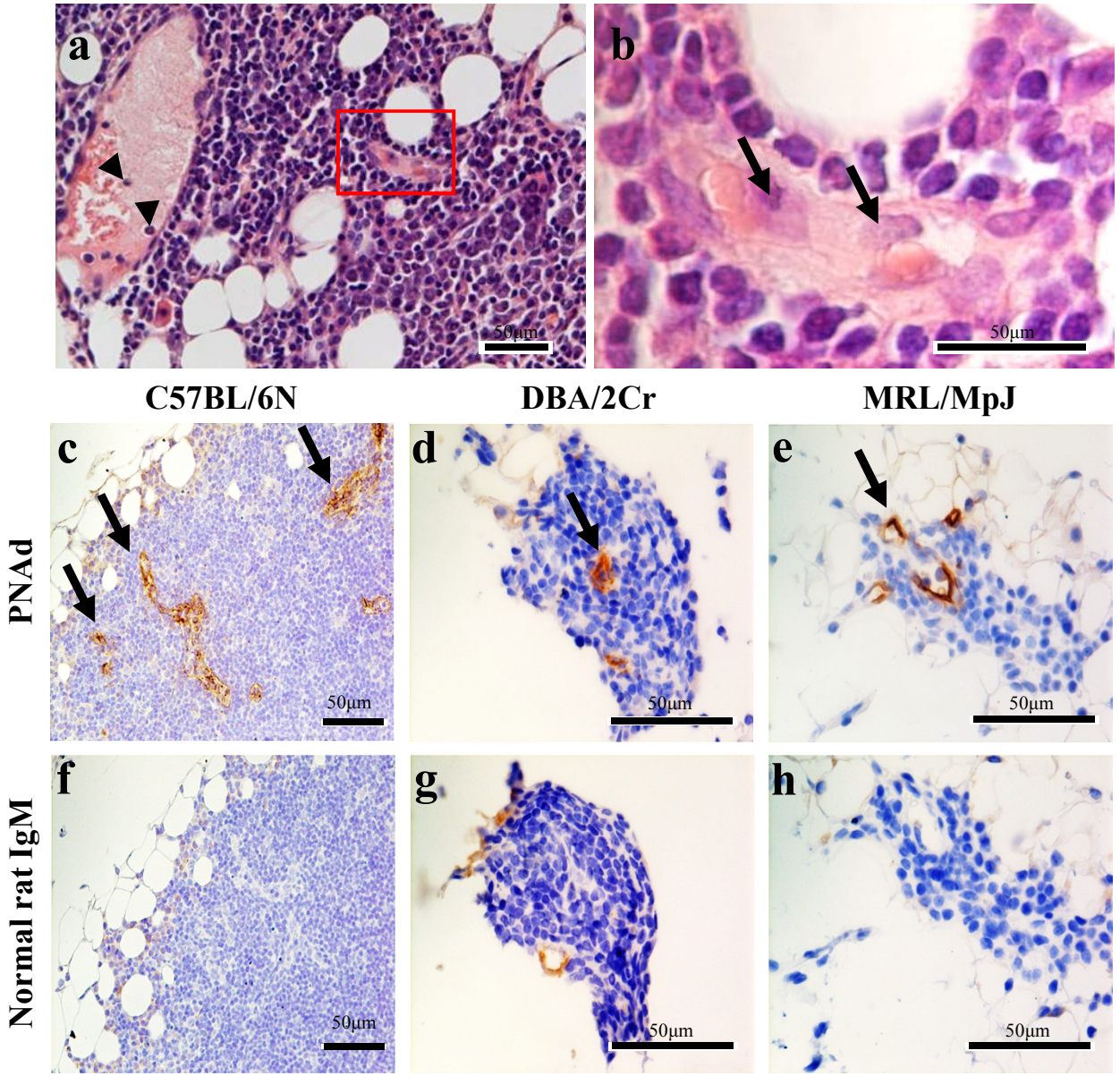
a
b
50μm
50μm
C57BL/6N
DBA/2Cr
MRL/MpJ
PNAd
Normal rat IgM
c
d
e
f
g
h
50μm
50μm
50μm
50μm
50μm
50μm

Figure 5.

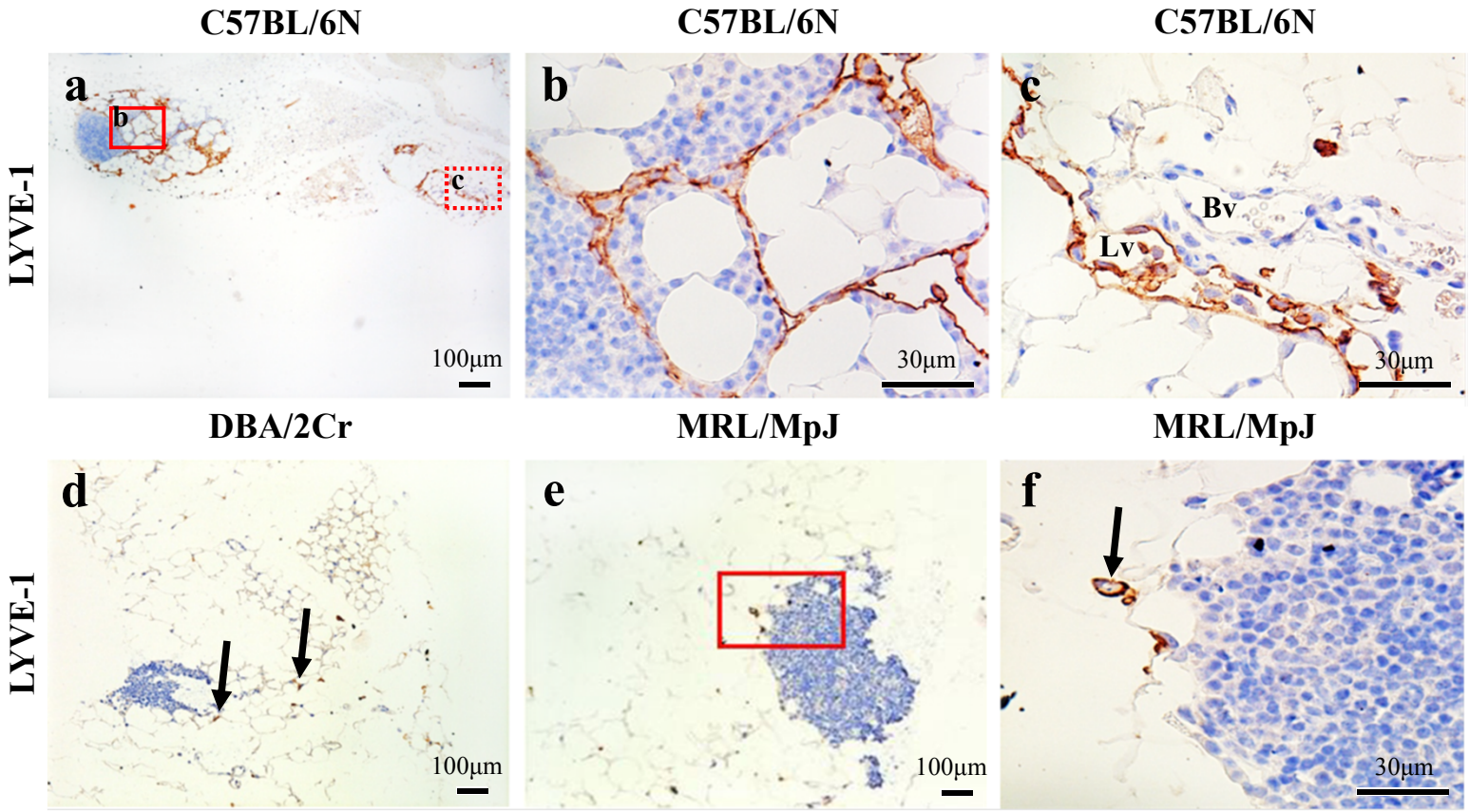
C57BL/6N
C57BL/6N
C57BL/6N
LYVE-1
a
b
c
100μm
b
30μm
c
Bv
Lv
30μm
DBA/2Cr
MRL/MpJ
MRL/MpJ
LYVE-1
d
100μm
e
100μm
f
30μm

Figure 6.

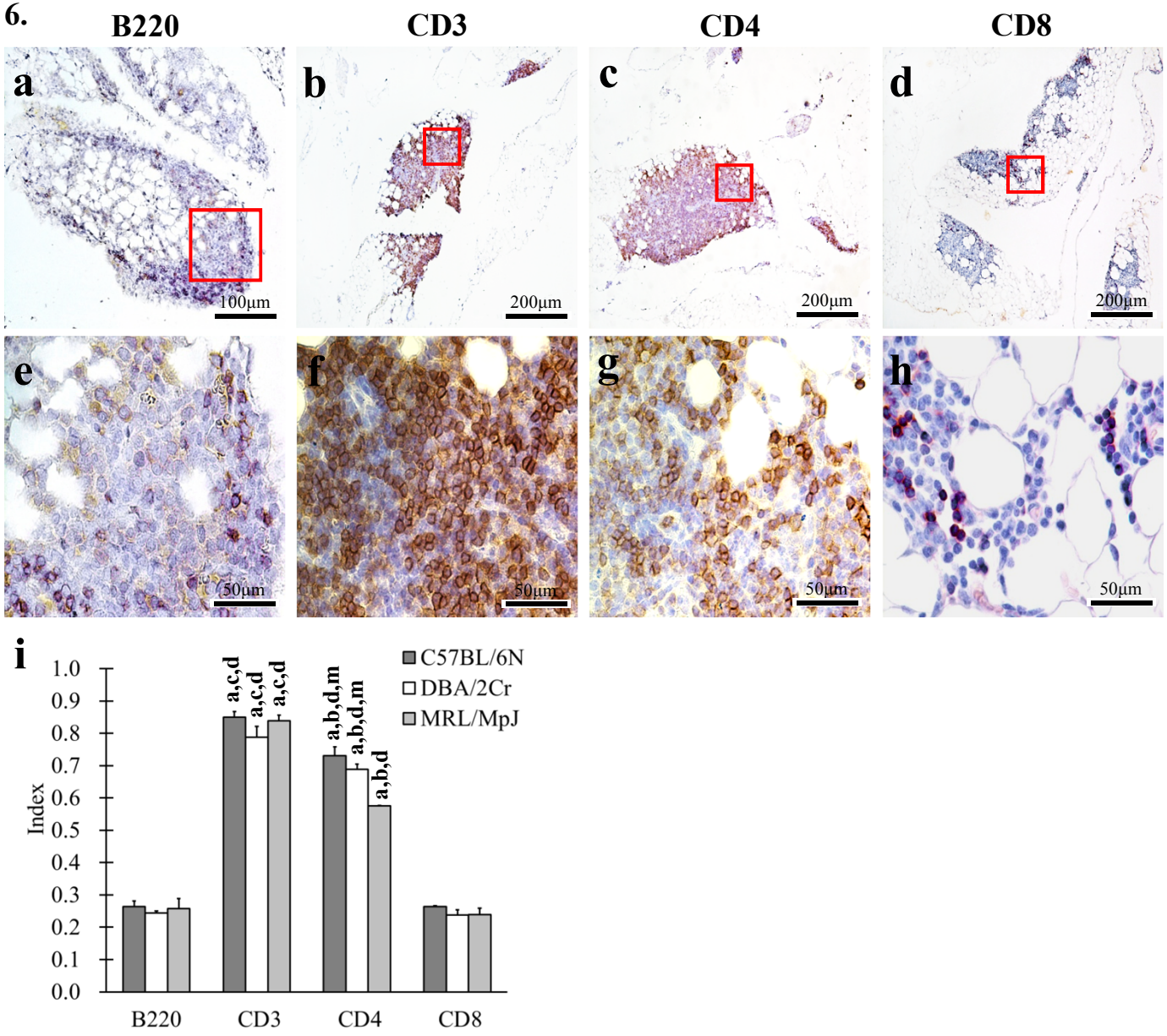
B220
CD3
CD4
CD8
a
b
c
d
100μm
200μm
200μm
200μm
e
f
g
h
50μm
50μm
50μm
50μm
i
C57BL/6N
DBA/2Cr
MRL/MpJ
Index
1.0
0.9
0.8
0.7
0.6
0.5
0.4
0.3
0.2
0.1
0.0
a,c,d
a,c,d
a,c,d
a,b,d,m
a,b,d,m
a,b,d
B220
CD3
CD4
CD8

Figure 7.

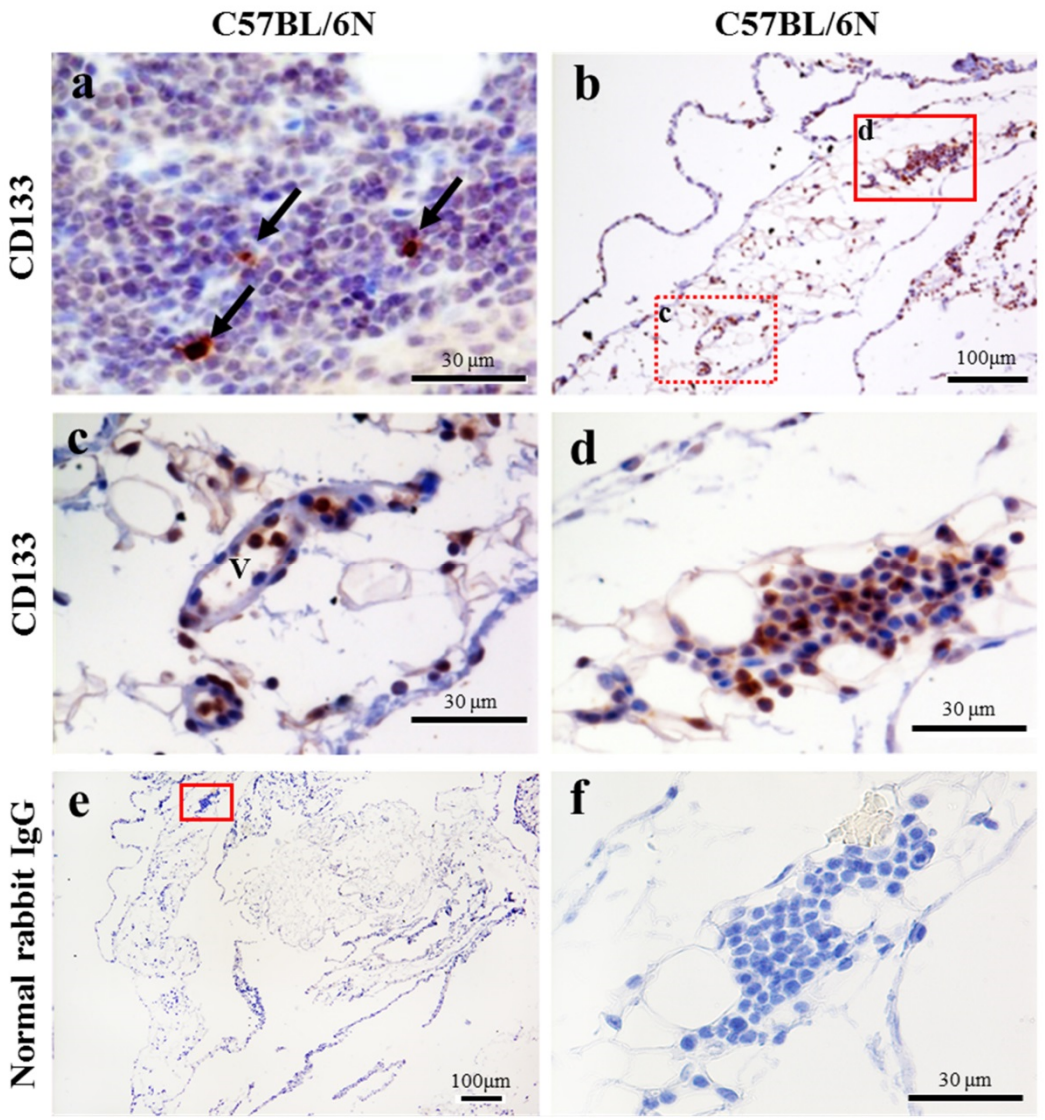
C57BL/6N
C57BL/6N
CD133
CD133
Normal rabbit IgG
a
b
c
d
e
f
30 μm
100μm
V

Figure 8.

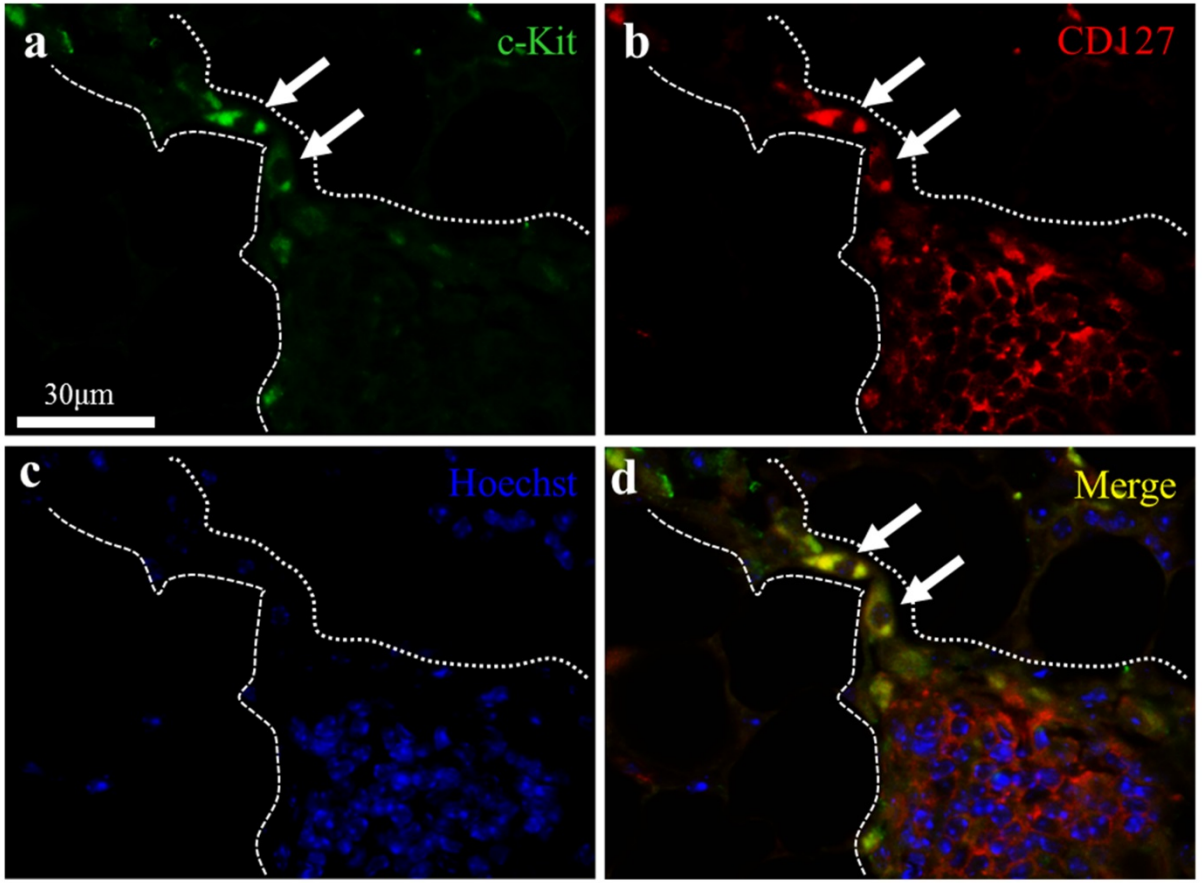

Figure 9.

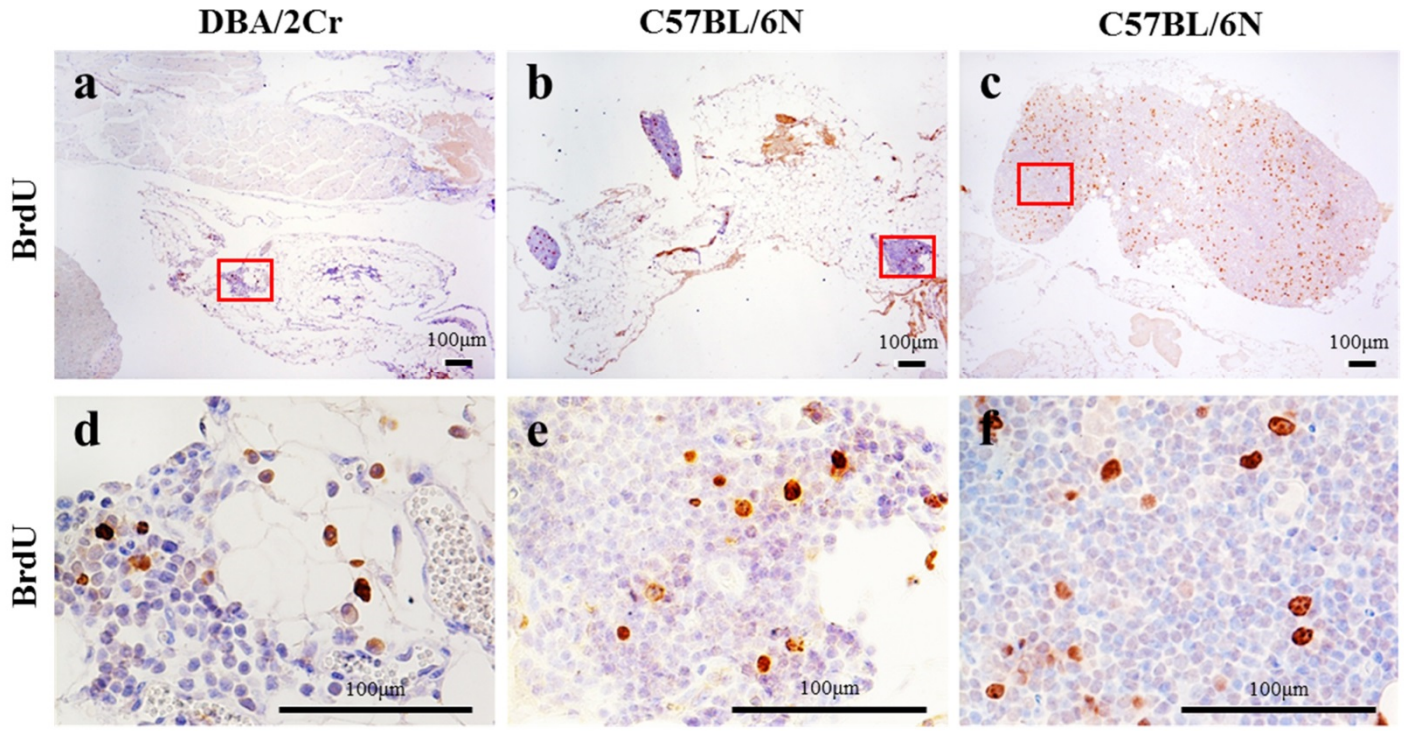
DBA/2Cr
C57BL/6N
C57BL/6N
BrdU
BrdU
a
b
c
d
e
f
100μm
100μm
100μm
100μm
100μm
100μm